AD_____

Award Number:

W81XWH-04-1-0034

TITLE:
Enhanced Ultrasound Visualization of Brachytherapy Seeds by a Novel Magnetically Induced Motion Imaging Method

PRINCIPAL INVESTIGATOR:
Stephen McAleavey, Ph.D.

CONTRACTING ORGANIZATION:
University of Rochester, Rochester, NY 14627

REPORT DATE:
October 2009

TYPE OF REPORT:
FINAL

PREPARED FOR: U.S. Army Medical Research and Materiel Command
                Fort Detrick, Maryland 21702-5012

DISTRIBUTION STATEMENT:

   X   Approved for public release; distribution unlimited

REPORT DOCUMENTATION PAGE

Form Approved
OMB No. 0704-0188

Public reporting burden for this collection of information is estimated to average 1 hour per response, including the time for reviewing instructions, searching existing data sources, gathering and maintaining the data needed, and completing and reviewing this collection of information. Send comments regarding this burden estimate or any other aspect of this collection of information, including suggestions for reducing this burden to Department of Defense, Washington Headquarters Services, Directorate for Information Operations and Reports (0704-0188), 1215 Jefferson Davis Highway, Suite 1204, Arlington, VA 22202-4302. Respondents should be aware that notwithstanding any other provision of law, no person shall be subject to any penalty for failing to comply with a collection of information if it does not display a currently valid OMB control number. **PLEASE DO NOT RETURN YOUR FORM TO THE ABOVE ADDRESS.**

1. REPORT DATE (DD-MM-YYYY) 01-10-2009	2. REPORT TYPE Final	3. DATES COVERED (From - To) 1 APR 2004-30 SEP 2009
4. TITLE AND SUBTITLE Enhanced Ultrasound Visualization of Brachytherapy Seeds by a Novel Magnetically Induced Motion Imaging Method		5a. CONTRACT NUMBER
		5b. GRANT NUMBER W81XWH-04-1-0034
		5c. PROGRAM ELEMENT NUMBER
6. AUTHOR(S) Stephen McAleavey, Ph.D. E-Mail: stephenm@bme.rochester.edu		5d. PROJECT NUMBER
		5e. TASK NUMBER
		5f. WORK UNIT NUMBER
7. PERFORMING ORGANIZATION NAME(S) AND ADDRESS(ES) AND ADDRESS(ES) University of Rochester Rochester, NY 14627		8. PERFORMING ORGANIZATION REPORT NUMBER
9. SPONSORING / MONITORING AGENCY NAME(S) AND ADDRESS(ES) U.S. Army Medical Research and Materiel Command Fort Detrick, Maryland 21702-5012		10. SPONSOR/MONITOR'S ACRONYM(S)
		11. SPONSOR/MONITOR'S REPORT NUMBER(S)

12. DISTRIBUTION / AVAILABILITY STATEMENT
Approved for Public Release; Distribution Unlimited

13. SUPPLEMENTARY NOTES

14. ABSTRACT
No abstract provided.

15. SUBJECT TERMS
No subject terms provided.

16. SECURITY CLASSIFICATION OF:			17. LIMITATION OF ABSTRACT	18. NUMBER OF PAGES	19a. NAME OF RESPONSIBLE PERSON USAMRMC
a. REPORT U	b. ABSTRACT U	c. THIS PAGE U	UU	26	19b. TELEPHONE NUMBER (include area code)

Standard Form 298 (Rev. 8-98)
Prescribed by ANSI Std. Z39.18

Table of Contents

Introduction

We have devised a method called Magnetically Induced Motion Imaging (MIMI) for identifying brachytherapy seeds in ultrasound images. Ultrasound guided brachytherapy is a common treatment for prostate cancer. The overall goal of this project is the unambiguous identification and accurate localization of brachytherapy seeds with ultrasound. Accurate determination of seed location is critical in delivering the correct dose distribution to the prostate. Automatic seed segmentation and real-time dose planning are enabled by this technique. Furthermore, the technique enables ultrasound to replace CT for post-implant evaluation, by providing a mechanism by which implanted seeds may be reliably identified by ultrasound. The proposed research will investigate and optimize the materials, instrumentation and algorithms for MIMI, to develop simulation, analytic and phantom methods to explore the relevant phenomena, and to conduct clinically realistic evaluations of the method.

Body

This report documents activities related to this grant for the period of April 1 2004 to March 30 2009. The grant was originally awarded to the PI April 1 2004 at Duke University. The work was suspended the following month when the PI transferred to the University of Rochester. Work resumed at Rochester June 2005. The PI applied for and was granted a no-cost extension.

The Statement of Work identifies the following tasks:

Task 1. Modeling of seed electromechanics (Months 1-18)
      A) Propose magnetic core geometry
      B) Develop finite-element model of magnetic seed core for electromagnetic simulation
      C) Solve for seed forces as a function of field strength, orientation and gradient
      D) Iteratively modify core design to maximize induced force given a constant-volume constraint

Task 2. Modeling of seed-tissue mechanics (Months 6-24)
      A) Develop finite-element mesh of seed and tissue
      B) Solve for steady-state vibration amplitude over 50-500Hz band
      C) Calculate vibration amplitude of seed vs. frequency
      D) Find iso-amplitude contours within tissue as a function of vibration frequency

Task 3. Seed detection algorithm development (Months 12-36)
      A) Simulate ultrasound RF echoes from seed and tissue vibrating as determined in Task 2 for varying seed-beam angle
      B) Evaluate motion detection and clutter suppression methods
      C) Determine vibration frequency that provides maximum spatial resolution

Task 4. In-vitro implementation (12-36)
      A) Fabricate or procure model seeds based on core design developed in Task 1
      B) Procure prostate phantom
      C) Implant seeds and clutter targets in prostate phantom
      D) Capture RF echo data and generate seed images using the algorithm of Task 3
      E) Implant seeds in excised animal tissue samples and image using the algorithm of Task 3

The accomplishments related to each task are described below; parts of this report reprise material from previous annual reports.

Task 1: Modeling of seed electromechanics

The goals of this task were achieved. A parametric model for seed core geometry was developed and evaluated using finite-element modeling software. An "ideal" shape was determined by maximization of magnetic torque over the range of possible core shapes allowed by the parametric model. Our results indicated that a simple cylinder generates 90% of

the torque associated with the ideal shape while being much easier to manufacturer. Below is a brief summary of the details associated with this task.

Finite element modeling of magnetic cores and associated forces was performed in Comsol Multiphysics (Comsol AB). FEMLAB was selected for its ability to run on multiple platforms, low cost, and relatively low learning curve for student researchers.

Initial 3D finite-element models focused on two seed magnetic-core geometries, an ellipsoid and a rod capped by two semi-hemispheres. These initial models were selected to allow straightforward comparison to analytical torque models [Jones]. The seed cores are modeled as being of iron with an isotropic relative permeability of μ_r=4000. The models subject the seed to a unit-strength uniform field. All torques induced in the seeds are due to the physical anisotropy of the seeds; material effects are ignored by selecting an isotropic material permeability so we can concentrate on seed geometry.

The torque exerted on the seed was calculated by the Maxwell Stress Tensor method [Wangsness]. The net torque about a given axis is computed by integrating the cross product of the tensor and lever arm length over the surface of the seed [Comsol]. We found the torque is proportional to $\sin(2\theta)$, as expected [Jones]. Both seeds have identical volumes (0.0013mm^3), yet the rod shaped core generates ~1.75 times the torque of the ellipsoidal core. This result confirms our initial hypothesis that torque would be sensitive to seed core shape and encourages us to further explore variations in torque with geometry variations.

Simulation of seed electromagnetic forces continued with the goal of determining an optimum core geometry.   Our goal is to find the magnetic core shape that maximizes this torque subject to constraints on volume, maximum length, and maximum width imposed by the shape of a standard brachytherapy seed. In carrying out this work we took advantage of an electric-magnetic duality. The problem of estimating torque on a linearly magnetizable due to an applied magnetic field is equivalent to the problem of estimating torque due to an electric field on a dielectric particle. Just as the magnetic brachytherapy seed cores experience a torque when placed in a magnetic field due to induced magnetization, a non-polarized dielectric particle of isotropic material suspended in an electrostatic field experiences a torque by induced polarization due to shape anisotropy.

We employed two finite element models to find a torque-maximizing core shape. In our first model, cores were modeled as a pair of symmetric frusta joined at their faces to form tapered, rod-like shapes. The radii of the rod ends were equal and the radius at the particle's waist adjusted to maintain constant volume. The torque-maximizing shape is strongly dependent ε_r, the particle's relative permittivity, low values favoring mass concentration near the waist of the particle and high values favoring concentration of mass near the ends. A more detailed model was created as a stack of nine frusta subject to the same symmetry and constant-volume constraints. For high relative permittivity material ($\varepsilon_r = 4000$), a shape with mass concentrated at the ends of the particle, gives the highest torque.

The details of the modeling are presented in Appendix A1 in the publication "Shape optimization of elongated particles for maximum electrical torque," presented at the 2007 Electrostatic conference of the Institute of Physics. The key result of this work is that for highly magnetizable materials, as would be used for the proposed brachytherapy cores, there is a slight advantage in torque to be gained by distributing the core material towards the end of the seed. The maximum improvement compared to a simple cylinder, on the order of 10%, may not be sufficient in practice to justify the cost of shaping the core. A second interesting result, albeit of limited utility in the brachytherapy seed problem, is that the torque maximizing shape is a function of the magnetic permeability (electric permittivity) of the seed core. In summary, the goals of developing a finite element model of the torque on a ferromagnetic seed core due to an imposed magnetic field and finding the optimum core shape compatible with a practical brachytherapy seed were achieved.

Task 2: Modeling of seed-tissue mechanics
The goal in this task was to understand the vibration response of a seed in tissue subject to magnetically generated torque. We developed a finite-element model for a seed embedded in tissue and calculated the response to a sinusoidally varying torque on the seed. Tissue was modeled as a viscoelastic solid, where the shear modulus G is time dependent

$$G(t) = G_\infty + (G_0 - G_\infty)e^{-\beta t}$$

where G_0 is 670Pa, G_∞ is 67, and β is 100μs. A 50kPa bulk modulus and a density of 1g/cm^3 was applied for the tissue. The seed was modeled as a rigid bar with a density of 10g/cm^3. The mesh was 37.5 x 25 x 10 mm with an isotropic element size of 0.375mm. A weak resonance (Q of approximately 1.7) was found for the seed-tissue system at a frequency of approximately 310Hz.

Task 3: Seed detection algorithm development

The goal of this task was to develop an integrated model that incorporated magnetic torque, seed vibration and shear wave propagation in tissue, and ultrasound scattering and imaging to allow simulation of entire seed imaging process. Tissue properties, seed core geometry, and ultrasound scanner parameters are all controllable within this simulation. The output of the model is simulated ultrasound RF echo data. The simulated data were then used to evaluate and refine seed detection algorithms based on the vibration-induced phase shift in the ultrasound echo. We were successful in completing this task.

Code for simulating the ultrasound from vibrating seeds and tissue has been developed and tested. Tissue is modeled as a uniform scattering medium by a set of randomly positioned point targets of equal echogenicity. These points are uniformly distributed within a specified volume, with a density of 10 scatterers per resolution cell. These point locations are taken as the initial, pre-displacement scatterer positions. Displacement vector field data from the finite-element simulations are used to reposition the scatterers at several (3-10) time steps within a vibration cycle. For each scatterer in the phantom, the eight surrounding mesh points are determined. The displacement components of the scatterer are linearly interpolated from the displacement vectors at each mesh point. Scatterer motion in all three dimensions is simulated in this model.

A simulated RF ultrasound echo is generated at each FEM timestep using Field II, a linear acoustic scattering simulator [Jensen]. A Siemens Antares VF10-5 probe was modeled as the imaging transducer; other transducers and scan geometries may be easily applied to the model. At each timestep, scanning of the repositioned scatterers is simulated to produce a synthetic RF signal. The process is repeated for every time step in the finite-element simulation. It should be noted that this code has proven useful in other research. In particular, it was adapted and applied to ARFI imaging simulation [Palmeri].

Details of the seed detection algorithms and in-vitro implementation of these methods were published (Appendix A2) "Magnetically Vibrated Brachytherapy Seeds: Ferromagnetic Core Models and Image Reconstruction Methods." The principle research results are the development of a compounding technique to reduce "comet-tail" ringdown artifacts in seed images, and a directional blurring method to link seeds together. A summary of these methods is presented here.

As shown in Figure 4 of Appendix A2, a seed rocking about its center naturally has the greatest vibration amplitude at its ends.   An image of vibration amplitude thresholded to a particular value will result in a "dumbbell" shape seed image. Ideally, the detected shape would completely enclose the seed and approximate its shape.   The directional blurring methods described uses the phase of the vibration signal to determine the orientation of the seed and link opposite seed ends, resulting in a seed image which encloses the seed and more accurately describes its shape and orientation.

A second imaging artifact is the "ring-down" or "comet-tail" artifact due to ultrasound reverberation within the seed. The result of this reverberation is a tail in the image that proceeds away from the seed in the direction of the ultrasound beam. This tail complicates image segmentation and interpretation and could result in a mistaken estimate of seed orientation.

The compounding technique described in the paper combines seed images obtained from multiple angles to suppress the ring down artifact. This method uses the principle that, while the tail will change position as the ultrasound beam is steered, the seed itself remains fixed. We acquire seed images at two different beam angles and threshold to create a pair of binary images. A final seed image is created by calculating the pixelwise logical AND of each image. The comet tails, with their different position in each image, are suppressed, while the seed itself is unaffected. This method and result is described in section IIIC of Appendix A2 and illustrated in figures 4-7.

Additional simulations were performed to evaluate detection of seeds at a variety of orientations to the ultrasound transducer, and to compare the MIMI and B-mode detection of the seeds. Simulations were conducted with the seed major axis in the scan plane. The simulations were performed using the integrated simulation described previously. These

simulations do not include seed reverberation effects, but do accurately model the change in backscatter as a function of seed/beam angle. Seeds were modeled as a dense (~1/2 λ between scatterers) collection of point scatterers, while the background was modeled as a diffuse collection of randomly distributed point scatterers. The same arrangement of scatterers was used for each simulation, with the entire collection of scatterers rotated through an angle of 0-90 degrees.

The simulated seed was scanned from 0 to 90 degrees (parallel to perpendicular to the transducer face) in 10 degree increments. The resulting scans are shown in figure 2. As expected, the echo from the seed decreases rapidly as its angle to the transducer increases. For angles of greater than 20 degrees the seed is difficult to detect, and for angles greater than 30 the seed is invisible in B-mode images. These images simulate a seed in a homogenous speckle environment. In the presence of other structures (calcification, air bubbles due to needle insertions) one would expect even greater difficulty in distinguishing seeds.

Simulations of MIMI imaging of seeds was performed through a combination of finite element simulation of seed/tissue motion and ultrasound scattering simulation. Comsol Multiphysics [Comsol] was used to simulate motion of a seed embedded in tissue. Tissue was modeled as a linear elastic material with a shear modulus of 10kPa and density of 1000kg/m^3. The seed was modeled as a 5mm long, 1mm diameter solid steel cylinder. A sinusoidally varying torque of 200Hz frequency was applied to the seed, and the transient solution calculated until a steady state was achieved. The calculated displacements from the FEM within the scan plane (lateral and axial) was applied. Displacement amplitude was scaled to a maximum of 0.5 λ at the seed ends. The seed and tissue were imaged with the seed at 0, 10, 20, 30, and 90 degrees to the transducer face. The scatterers were displaced and scanned at 11 time steps within a single cycle of steady-state oscillation to simulate Doppler scanning with a 20kHz PRF. The motion of the seed and tissue was tracked by windowed cross-correlation [Palmeri], with a window length of 2.5 μs (12.5 λ).

Images of estimated displacement amplitude from the RF echo sequence are shown in figure 3 for 0-90 degree scan angles. As can be seen from the figures, the seed remains visible over the entire range of angles, in contrast to the B-mode images of the seed.   Figure 4 shows the same images presented with a larger dynamic range, showing that it is possible to more precisely localize the seed ends over a range of angles. These simulations confirmed the hypothesis that seeds remain visible in MIMI images, even when the seed is invisible in the corresponding B-mode image, due to the induced motion of the surrounding tissue. Tissue has an omni-directional scattering characteristic. The Doppler signal (echo displacement signal) imposed on the tissue by seed motion can thus be detected even when the seed itself is not visible.

Matching in vitro imaging of a seed in a tissue-mimicking phantom was performed to verify the model. Figure 5 shows images of a seed at 0 and 90 degrees to the transducer face. The power Doppler signal due to the seed is visible in both orientations, while the seed itself is invisible B-mode at the 90 degree orientation. Scans were performed for applied magnetic field frequencies of 100/150Hz, 500Hz, and 1000Hz. Increasing the drive frequency resulted in a more localized Doppler signal. While this is due in part to the reduce magnetic field developed at high frequency due to coil inductance, the higher frequency shear waves induced are also damped more rapidly by the tissue-like material, resulting in a more tightly localized seed. Both low and high frequency seed drive are useful – low frequency for finding misplaced seeds, and high frequency for precise localization of a seed of known position.

A method was developed for detecting and compensating for physiological tissue motion and transducer movement, i.e. motion not due to seed vibration. Such compensation is necessary, as motion not related to seed vibration will produce a Doppler clutter signal that could potentially obscure seeds. This method relies on the fact that physiological and transducer motion is relatively slow and induces a low frequency Doppler signal, on the order of 10's of Hz. In contrast, the seed vibration is controllable and typically on the order of 100's of Hz to a few kilohertz.

In our clutter suppression method, illustrated schematically in figure 6, we estimate the low frequency component of tissue motion. This low-frequency component is illustrated in figure 5a, where a slow gross motion away from the transducer results in a given echo arriving progressively later after pulse transmission. This gross motion is estimated using standard Doppler [Kasai] methods and fit to a constant velocity. A "motion-compensated" Doppler ensemble is then formed by time shifting each echo by the amount estimated. The remaining Doppler ensemble contains only signal due to seed vibration, or high-frequency noise. This method has produced >10db suppression of Doppler clutter in our measurements.

In summary, the goals of this Task were accomplished. An integrated simulation model was developed, incorporating the magnetic, tissue mechanical, and ultrasound scanning elements of the seed imaging process. The simulated data was used to evaluate seed detection algorithms, including physiological motion suppression methods. Techniques for reducing

image artifacts, including "comet-tail" artifacts, were developed and published. Finally, the simulations were confirmed by in-vitro scanning.

Task 4: In-vitro implementation

We have created several tissue-mimicking phantoms in which to embed seeds for scanning and RF Doppler data collection. These phantoms are fabricated of polyvinyl-alcohol (PVA) cryogel following the procedure outlined in [Surry2004] with the addition of 60g powdered graphite per liter of PVA solution to improve backscatter characteristics of the phantoms. PVA cryogel is a convenient material for these phantoms because their stiffness may be varied readily; repeated freezing and slow thawing of the phantoms increases their stiffness. Thus, phantoms with a relatively wide range of stiffness (Young's Modulus of ~2-40kPa) may be prepared from a single material mixture, providing uniform ultrasound characteristics between phantoms.

Seeds embedded in these phantoms roughly match the rod model in task 1. The phantoms were scanned with the Siemens Antares scanner. A VF10-5 7MHz linear array transducer was used. Volumetric scans were performed with a 3-axis positioning system (Newport Corporation). The translation stage and scanner were controlled via a custom Matlab script. The transducer was stepped 1mm in the out-of-plane direction. Screen captures and RF data were grabbed at each step. RF Doppler data was captured via the Siemens Antares Ultrasound Research Interface (URI) software and imported into Matlab for analysis (see Task 3).

Color Doppler data was used to perform 3D reconstructions of the seeds. Figure XX is a 3D isosurface reconstruction of a single seed in tissue. The two vibration lobes are due to the rocking motion of the seed in response to the magnetic field, which results in the tips of the seed moving most, with the center moving little. The isosurface reconstruction from in vitro Doppler data agrees very well with our previous simulations [McAleavey], which showed a distinct "dumbbell" shape to the vibration amplitude isosurface.

Key Research Accomplishments
- Finite-element model of magnetic force on ferromagnetic seed
- Determination of optimal ferromagnetic core geometry
- Demonstration of insensitivity of Doppler signal to ultrasound frequency and beam angle
- *In-vitro* 3D reconstruction of vibration field
- Coupled magnetic/tissue mechanical/ultrasound simulation model
- Simulated and *in-vitro* demonstration of seed detection at arbitrary orientations
- Development and demonstration of filtering algorithms to enhance seed contrast and suppress physiological motion

Reportable Outcomes:

Conference Presentation with Paper
(1) McAleavey S, Jones TB, Green N. "Shape Optimization of Elongated Particles for Maximum Electrical Torque," 12th International Conference on Electrostatics, Institute of Physics UK., Dec 2008. Journal of Physics Conference Series 142

(2) McAleavey S, White S, Menon M. "Magnetically Vibrated Brachytherapy Seeds: Ferromagnetic Core Models and Image Reconstruction Methods," IEEE International Ultrasonics Symposium, 2006, p 1103-1106

Conference Presentation with Abstract
(1) McAleavey S, Trahey GE. "Echo Signal Processing for Doppler Brachytherapy Seed Detection," International Symposium on Ultrasound Imaging and Tissue Characterization, Arlington, Virginia, 2003

Degrees Awarded:
- o Manoj Menon, Ph.D. Department of Biomedical Engineering, University of Rochester, 2010 "Resolution Metrics for Acoustic Radiation Force Imaging"

Funding:
- o *Quantitative Spatially Modulated Ultrasound Radiation Force Elastography*
  National Institutes of Health (NIBIB) (1 R21EB008724-02)
  P.I.: Stephen McAleavey
  July 2008-June 2010; $418,100

Employment:
- o Manoj Menon – Ultrasound Systems Engineer, Siemens Medical Solutions, Ultrasound Group, Issaqua, WA

Conclusions:

In this project we have addressed fundamental questions for the implementation of Magnetically Induced Motion Imaging for identifying brachytherapy seeds in ultrasound images. This research has investigated design of the ferromagnetic seed component, modeling of shear wave generation and echo phase modulation due to seed vibration, and signal processing methods for seed identification in images. Our modeling has determined that the primary force on the seed is a torque induced by shape anisotropy. We developed a finite-element based parametric search algorithm to determine the torque-maximizing ferromagnetic core shape.

In contrast to B-mode imaging, MIMI generates seed images that are relatively insensitive to seed/beam angle. This occurs because both the seed and surrounding tissue vibrate and modulate the echo signal. By virtue of its omni-directional scattering, the tissue Doppler signal is detectable even when the echo from the seed is undetectable. We have simulated MIMI imaging of seeds through a combination of finite element simulation of seed/tissue motion and ultrasound scattering simulation. A custom Matlab code was developed to translate displacements of the seed and tissue calculated though finite element simulation to the ultrasound scatterers used in the Field II simulation. We have developed an adaptive clutter-suppression method for eliminating signal due to for physiological tissue motion and transducer movement which would obscure seeds. Detection of the vibration induced echo phase shift allows unambiguous identification of the seeds.

The methods and technologies developed in this project have been applied to research outside the scope of this project. The technique has been applied by [Rogers] for the localization of ferrous shrapnel. The integrated finite-element tissue model and ultrasound simulation has been applied in other areas, including modeling ultrasound tracking of tissue response to acoustic radiation force impulses [Palmeri].

References

[Comsol]   *Electromagnetics Module User's Guide*, Comsol AB, 2004

[Jensen]   Jensen JA, "Field: A Program for Simulating Ultrasound Systems," *10th Nordic-Baltic Conference on Biomedical Imaging Published in Medical & Biological Engineering & Computing*, pp. 351-353, 34, Supplement 1, Part 1, 1996.

[Jones]   T. B. Jones, *Electromechanics of Particles*, Cambridge, 1995

[Kasai]   Kasai C, et al., "Real-Time Two-Dimensional Doppler Flow Mapping Using Auto-Correlation," *Acoustical Imaging: Proceedings of the International Symposium*, 13, pp 447-460, 1984

[McAleavey]   McAleavey SA, Palmeri M, Gracewski S, Trahey GE, "Ferromagnetic Brachytherapy seed motion in soft tissue: Models, measurements and ultrasound detection," *Proceedings of the IEEE Ultrasonics Symposium*, pp. 1575-1579, 2002

[Palmeri]   Palmeri ML, McAleavey SA, Trahey GE, Nightingale KR, "Ultrasonic tracking of acoustic radiation force-induced displacements in homogeneous media," *IEEE Transactions on Ultrasonics Ferroelectrics and Frequency Control* 53(7), pp 1300-1313, 2006

[Pyshnyia]   Pyshnyia MP, Kuznetsov OA, Pyshnayaa SV, Nechitailoa GS, Kuznetsova AA, "Synchronous ultrasonic Doppler imaging of magnetic microparticles in biological tissues," *Journal of Magnetism and Magnetic Materials,* 321(10), pp 1552-1556 2009

[Rogers]   Rogers AJ, Light ED, Smith, SW, "3-D ultrasound guidance of autonomous robot for location of ferrous shrapnel," *IEEE Transactions on Ultrasonics, Ferroelectrics and Frequency Control,* 56 (7), pp 1301–1303, 2009

[Surry]   K.J.M. Surry, H.J.B. Austin, A. Fenster, T.M. Peters, "Poly(vinyl alcohol) cryogel phantoms for use in ultrasound and MR imaging," Physics in Medicine and Biology 49, pp. 5529-46, 2004

[Wangsness]   R.K. Wangsness, *Electromagnetic Fields*, John Wiley and Sons, 1986
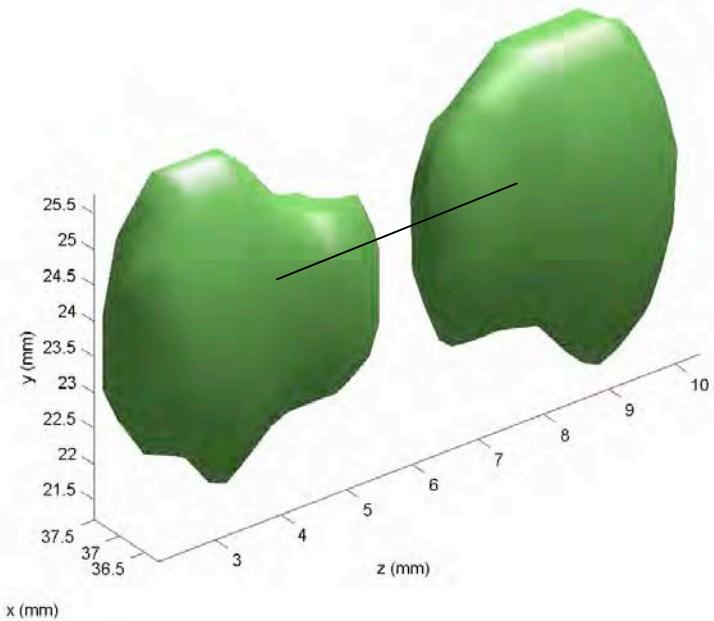
Figure 1. Isosurface volume rendering of seed and tissue vibration from Color Doppler data. The seed location is approximately denoted by the line. The transducer scan plane is the x-z plane. The volume reconstruction was performed by stepping along the y axis in 1mm steps. The lower out-of-plane resolution results in the greater apparent size in the y direction.
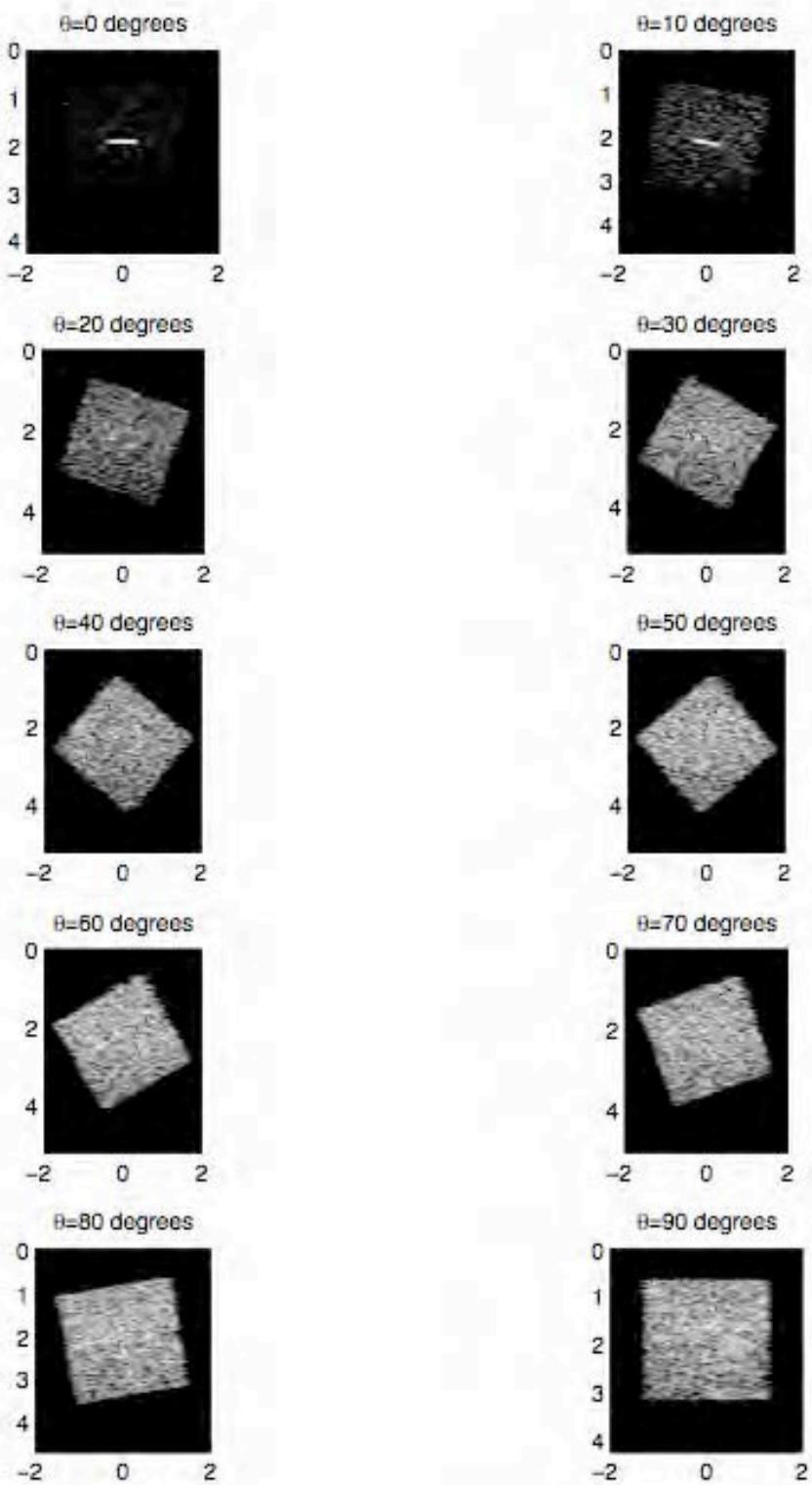
Figure 2. Simulated B- mode images of seeds at 0-90 degrees to the transducer face. Note that the seed is significantly obscured at 20 degrees, and invisible for angles of greater than 30 degrees. The system simulated is a 128 channel, 5MHz linear array with apodization and dynamic focusing
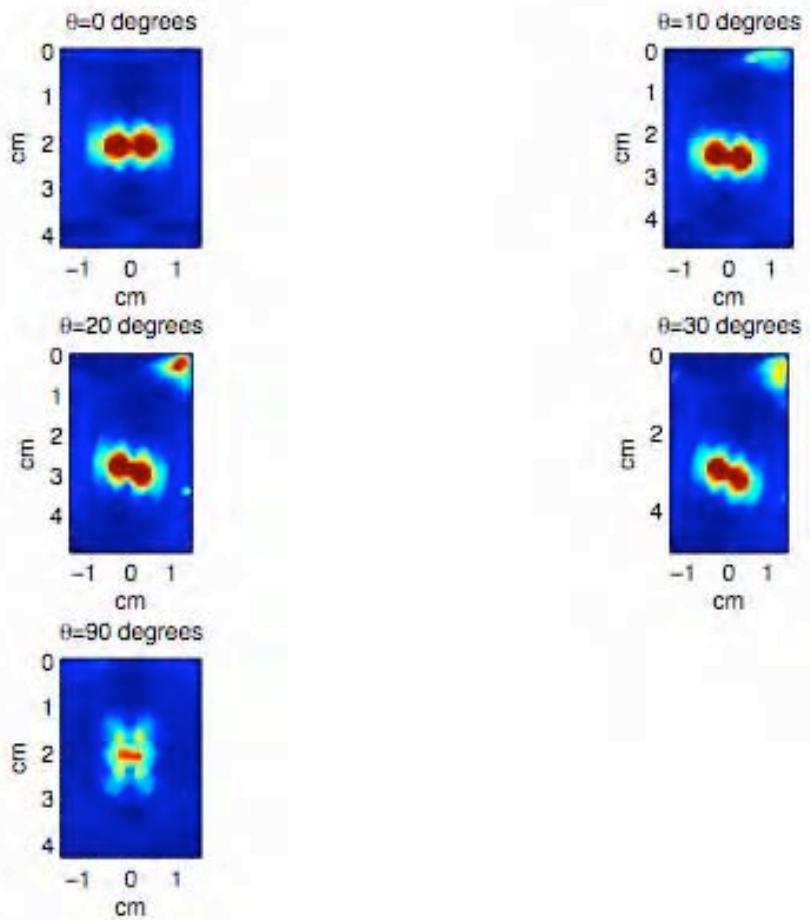
Figure 3. Motion amplitude estimates of seeds detected from simulated ultrasound echoes. Finite element simulations of seed and tissue motion in response to a sinusoidally varing magnetically induced force were used to displace scatterers in the ultrasound imaging model. The scatterers were rotated to orientations of 0, 10, 20, 30, and 90 degrees. In all cases, and in contrast with the B-mode images of Figure 1, the seed remains visible. Further, there is no speckle artifact in the motion estimate images to obscure the seeds.
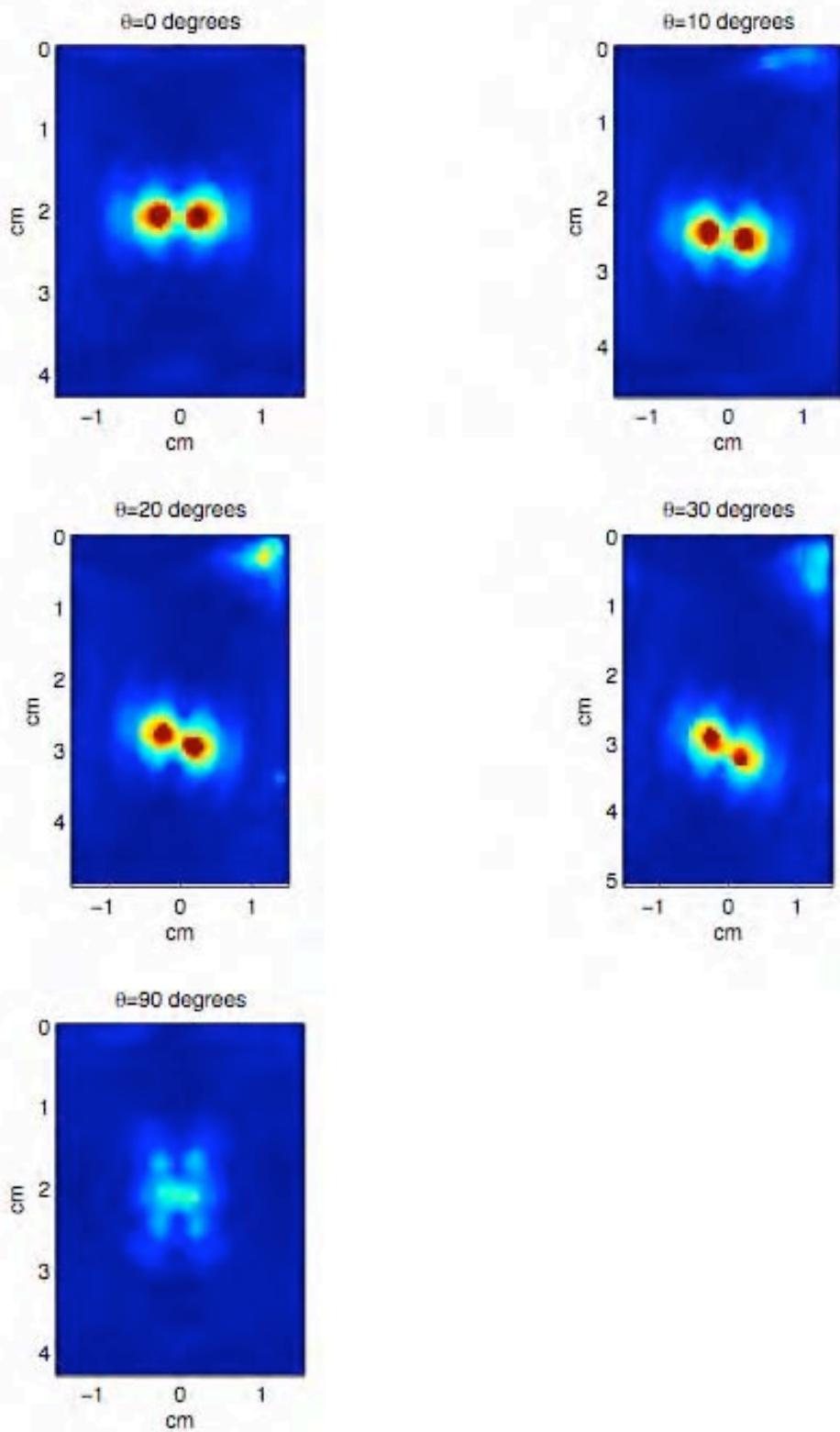
Figure 4. Motion estimate images of figure 2 presented with an expanded dynamic range. Here it is seen that the seed is still visible in all images, and that the seed location may be determined with greater precision than indicated in figure 2, with its saturated response.
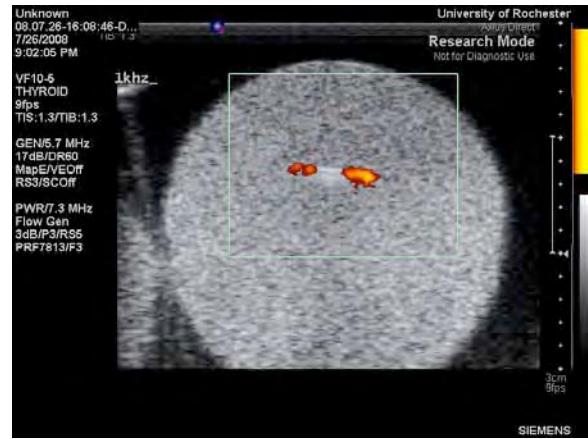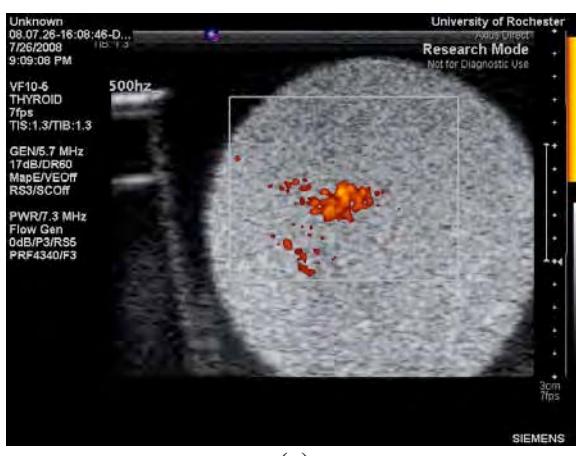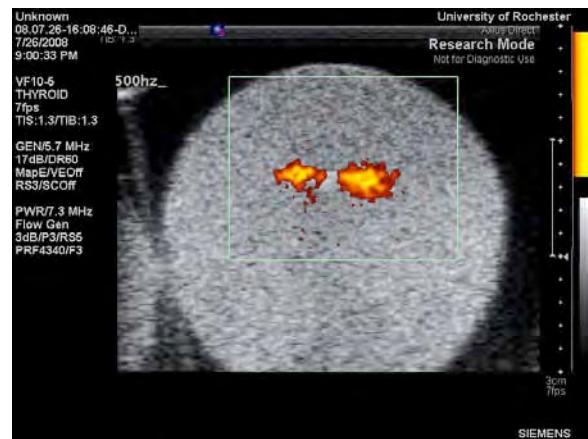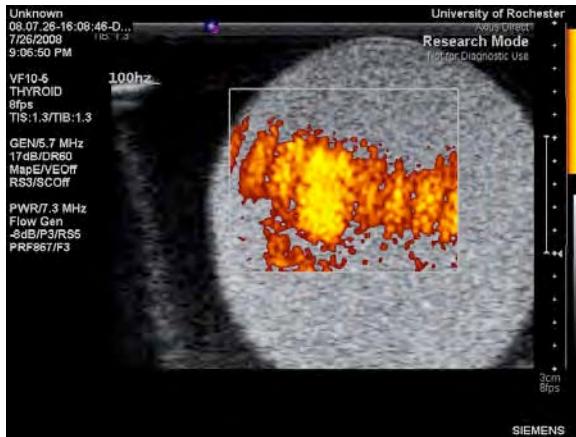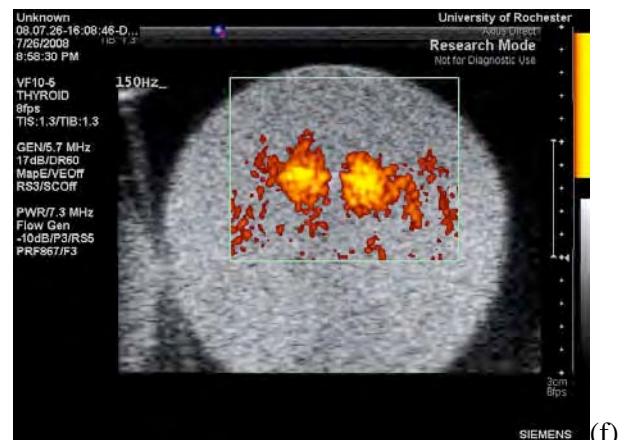
Figure 5. In vitro images of a seed in a tissue-mimicking phantom obtained using Power Doppler imaging. Seed orientation is 90 degrees (perpendicular to the transducer face) in (a,c,e) and 0 degrees (parallel to the transducer face) in (b,d,f). The seed is visible in both orientations, though it can be seen to be invisible in the 90 degree orientation in the B-scan (e.g. figure 4a) . Drive frequencies of 1000, 500, and 100Hz were used for the top, middle and bottom rows, respectively. The increased resolution available with higher drive frequency, and the larger area of induced motion at lower frequency, are evident.

Raw   Motion   Vibrating   'Static'
       compensate target

(a)   (b)   (c)   (d)
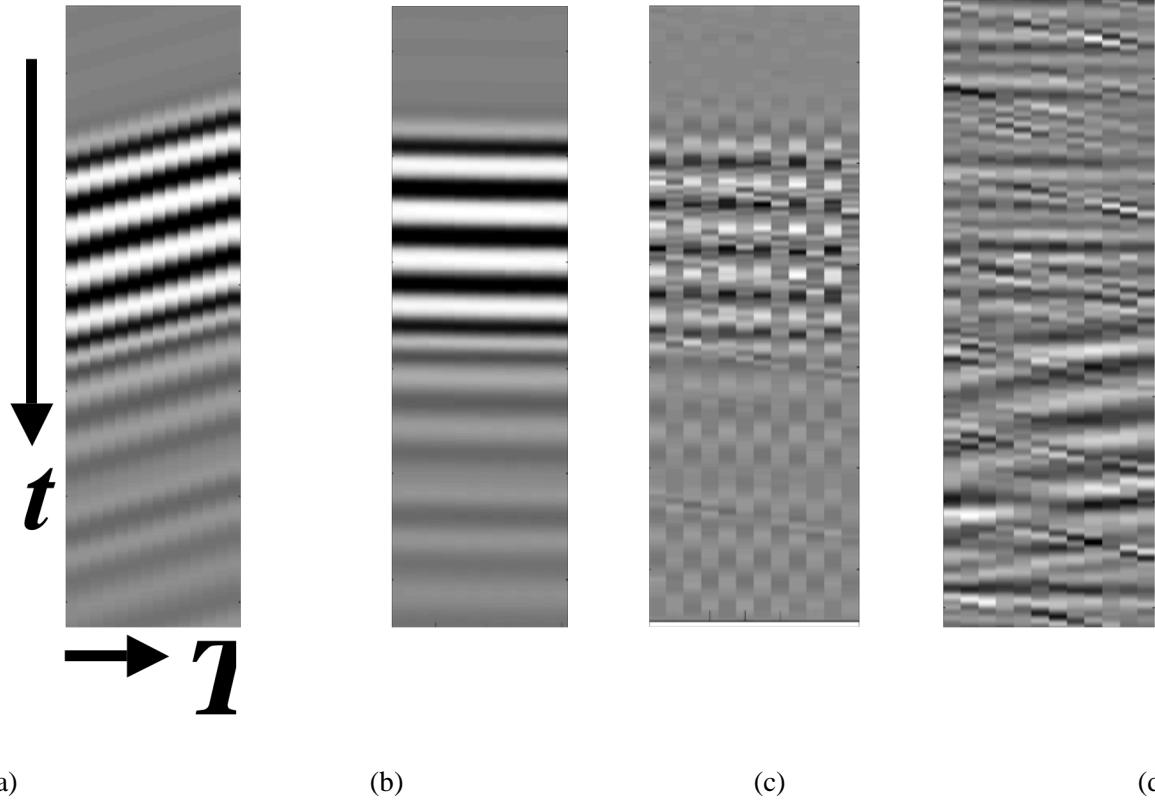
Figure 6. Steps in the clutter suppression algorithm. Raw Doppler data (a) is analyzed to determine a best-fit constant velocity estimate. The motion due to this constant velocity, assumed to be physiological or transducer motion, is subtracted from the Doppler ensemble by time shifting each echo (b). For a vibrating target (c), the vibration signal remains unaltered, while the static target (d) shows only noise. Stationary clutter suppression has been applied to (c) and (d).

Appendices:

A1:

McAleavey S, Jones TB, Green N. "Shape optimization of elongated particles for maximum electrical torque," 12th International Conference on Electrostatics, Institute of Physics UK., Dec 2008. Journal of Physics Conference Series 142

A2:

McAleavey S, White S, Menon M. "Magnetically Vibrated Brachytherapy Seeds: Ferromagnetic Core Models and Image Reconstruction Methods," IEEE International Ultrasonics Symposium, 2006, p 1103-1106

Shape optimization of elongated particles for maximum electrical torque

S A McAleavey[1*], T B Jones[1], and N Green[2]

[1]University of Rochester (USA) and [2]University of Southampton (UK)

[*]Correspondance: stephenm@bme.rochester.edu

Abstract: A non-polar particle of isotropic material suspended in an electrostatic field experiences a torque by induced polarization due to shape anisotropy. This torque is a strong function of shape and has a lower bound of zero in the limit of a sphere. Our goal has been to find the particle shape that maximizes this torque subject to constraints on volume, maximum length, and maximum width. In particular, the particle must fit within a cylinder of length to width ratio 11:1, and must occupy no more than 1/3 of the cylinder volume. We have employed a finite-element approach to search for this shape. In our first model, particles were modelled as a pair of symmetric frusta joined at their faces to form tapered, rod-like shapes. The radii of the rod ends were equal and the radius at the particle's waist adjusted to maintain constant volume. The torque-maximizing shape is strongly dependent ε_r, the particle's relative permittivity, low values favouring mass concentration near the waist of the particle and high values favouring concentration of mass near the ends. A more detailed model was created as a stack of nine frusta subject to the same symmetry and constant-volume constraints. For high relative permittivity material ($\varepsilon_r = 4000$), a shape with mass concentrated at the ends of the particle, gives the highest torque.

1. Introduction

It is well known that a non-polar particle of isotropic material in an electrostatic field experiences a torque due to induced polarization [1,2]. This torque is determined by the shape of the particle for a given field strength, particle volume, and permittivity. We have investigated the dependence of torque on shape and found that, when the geometry of the particle is constrained, the torque-maximizing shape is dependent on the permittivity of the particle.

The motivation for this work is the development of a method for imaging prostate brachytherapy seeds [3-4]. In this application a brachytherapy seed is a cylinder of length 4.5mm and diameter 0.8mm. The seeds contain a radioisotope and are implanted in the prostate as a cancer therapy. If made to vibrate in situ these seeds can be identified by Doppler ultrasound imaging methods. Vibration is induced by loading the seeds with a ferromagnetic core and subjecting the implanted seeds to an oscillating magnetic field. A design goal is to determine the core shape that produces the maximum vibration amplitude for a given volume of core material constrained to fit within a seed. When a linear magnetic model is used ($B=\mu_r\mu_0 H$) the electrostatic and magnetostatic problems are equivalent.

2. Theory

A non-polar isotropic particle of permittivity ε_2 and volume V in a fluid of permittivity ε_1 experiences a torque when an electric field E is applied. The torque is given by [1]

$$T = -VE^2 \frac{(\varepsilon_2 - \varepsilon_1)^2 (L_\parallel - L_\perp)}{\varepsilon_1 \left(1 + \frac{\varepsilon_2 - \varepsilon_1}{\varepsilon_1} L_\parallel\right)\left(1 + \frac{\varepsilon_2 - \varepsilon_1}{\varepsilon_1} L_\perp\right)} c_x c_z$$

where $L_\perp$ and $L_\parallel$ are functions of particle shape. The equivalent expression for an isotropic linear magnetic particle with permeability $\mu_r \mu_0$ is $T = -V\mu_0 H_0^2 \dfrac{\chi^2 (L_\parallel - L_\perp)}{(1 + \chi L_\parallel)(1 + \chi L_\perp)} c_x c_z$ where

$\chi = \mu_r - 1$. The two expressions are equivalent when $\varepsilon_2 = \mu_r \mu_0$ and $\varepsilon_1 = \mu_0$. Torque may be calculated conveniently for the case of spheroids where analytical solutions for $L_\perp$ and $L_\parallel$ are known [3]. For a prolate spheroid with major to minor axis ratio $r = a/b$, the spheroid eccentricity is defined as $e = \sqrt{1 - 1/r^2}$, $L_\parallel = \dfrac{1}{2r^2 e^2}\left(\ln\left(\dfrac{1+e}{1-e}\right) - 2e\right)$ and $L_\perp = (1 - L_\parallel)/2$. In the limit as r tends to infinity $L_\parallel \to 0$ and $L_\perp \to 1/2$ so that the limiting value of T is $VE^2 (\varepsilon_2 - \varepsilon_1)^2 / (\varepsilon_2 + \varepsilon_1)$ or $V\mu_0 H_0^2 \chi^2 / (2 + \chi)$ for the magnetic case.

The above expressions may be solved to calculate torque as a function of r normalized by the limiting torque value given above for a fixed V. Figure 1a is a plot of this solution for several values of relative permittivity $\varepsilon_r = \varepsilon_2 / \varepsilon_1$. For all values of ε_r the torque increases with particle elongation (increasing r). The increase in torque with r is most rapid for small values of ε_r implying particles with a high relative permittivity require a greater elongation to reach a fixed fraction of the maximum torque. This is depicted in figure 1b, a plot of the value of r required to reach 90% of the limiting torque value as a function of ε_r. Finally, figure 1c shows that the dependence of normalized torque as a function of V for a fixed length spheroid varies with ε_r. As expected, for a fixed length ellipsoid torque does not monotonically increase with V, as increasing volume transforms the spheroid into a sphere. Interestingly, the torque maximizing volume for a given major axis length depends on ε_r. Peak torque is achieved with a smaller volume for larger values of ε_r. Smaller values of ε_r favor a larger volume. These results suggested that the core shape sought for the brachytherapy seed will be dependent on μ_r, and that a torque maximizing particle shape in general will be dependent on ε_r.
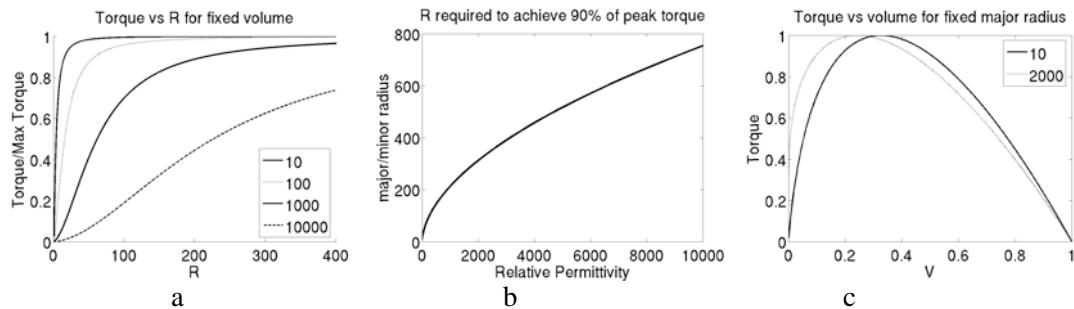

Figure 1. (a) Torque as a percentage of maximum value increases more slowly with particle length for a fixed volume as permittivity increase, as shown here for the indicated permittivities. (b) This same relationship shown as a function of permittivity. (c) For a spheroid of fixed major axis length, the volume, and hence shape, required to maximize torque depends on particle permittivity.

3. Methods

Torques on non-spheroidal particles were calculated using the Comsol Multiphysics finite element package (Comsol, Inc., Burlington, MA). Two models were considered. The first treats the particle as a stack of two frusta (truncated cones), as illustrated in figure 2a. The particles simulated had a fixed length 0.5cm and fixed volume. The ratio of end and center radii was varied to take the particles through a range of shapes from "bowtie" to "diamond," thus there was only one degree of geometrical freedom, $R=r_{end}/r_{center}$. The torque for each shape was calculated for ε_r values of 3, 30, 300, 3000. The torque was calculated by integrating the product of Maxwell Stress Tensor times the lever arm over the surface of the particle. Torques for the two-frusta particle were calculated for a range of R of 0.6 to 3.7.

A model composed of a stack of 9 frusta was constructed to search for a torque-maximizing shape with more degrees of freedom. The model had a fixed length of 0.5 cm and volume of 0.022π cm^3. As in the two-frusta model, lateral symmetry was imposed on the seed. Combined with the fixed volume constraint this model had two degrees of freedom, illustrated in figure 2b. Torques on this model were calculated for r1 and r2 ranging from 0.15 to 0.25, with r3 calculated to maintain constant volume for particular r1 and r2. In addition a guided optimization was sought using Matlab's **fmincon** function, which uses a sequential quadratic programming method to search for an optimum. A five-element model vector **y** described the seed radii at as many points over half its length, lateral symmetry and constant volume again being imposed. Calls to the Comsol solver returned torque values for a requested **y**, allowing the five-dimensional space to be searched efficiently.
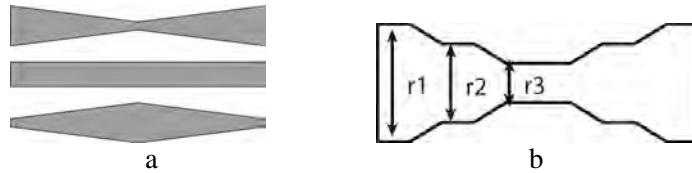

Figure 2. (a) Two and (b) nine frusta particle models. Constant volume is maintained for all.

4. Results

Figure 3a presents the calculated torque for the two-frusta normalized to the peak torque as a function of *R* for ε_r values of 3, 30, 300, and 3000. The results show the same trend suggested by the spheroid calculations. Particles with a low relative permittivity maximize their torque when their mass is concentrated toward their center. The mass of the torque-maximizing shape shifts towards the ends of the particle with increasing values of ε_r.

Figure 3b presents a contour plot of seed torques calculated for the model of figure 2b at the indicated values of r1 and r2, with r3 determined by the constant volume constraint, normalized to the maximum value calculated. The model had a relative permittivity of 3000. A cylinder of constant radius 0.21 generated a torque of 79% as great as the peak value, obtained with radii r1=0.220, r2=0.314, r3=0.194.   This result again shows torque is increased with mass concentrated towards the seed ends.

The constrained minimization search performed poorly, due to noise in the simulation arising from mesh changes with seed shape and numerical error. Future work on shapes with a greater number of degrees of freedom will require less noise-sensitive search methods.

5. Discussion

Both the analytical spheroid calculations and the finite element results indicate that the torque-maximizing shape varies as a function of permittivity. The total spheroid volume required for a

fixed major axis length particle to achieve maximum torque for a given material permittivity is not constant as shown in figure 1c. The finite element model showed that the torque maximizing two-frusta shape varied as a function of permeability/permittivity. Low values of ε_r favor a mass concentration near the particle waist, while high ε_r results in mass concentration at ends. The finite element model for the particle of figure 2b also favored an end-weighted shape consistent with its relatively high permittivity.

The torque optimization problem is challenging for particles whose shape has many degrees of freedom. The constrained search method was found to be susceptible to "noise" in the simulation due to variations in torque calculated for a given shape with different meshes. The variation in torque was on the order of 1-2% for different randomly generated meshes. This variation was often enough to confound the search algorithm. Search methods with better noise immunity, such as simulated annealing, may lead to better results.


a   b
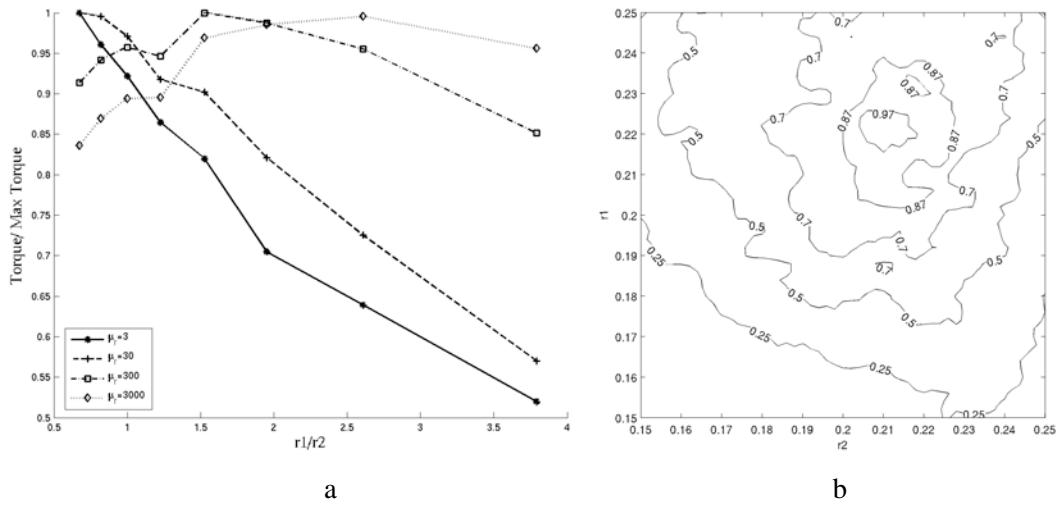
Figure 3. (a) Plots of the calculated torque for the particles of figure 2b for the indicated values of relative permittivity (3-3000) as a function of R. The peak torque moves to higher values of R as ε_r increases. (b) Contour plot of torques calculated for the particle of figure 2b for the radii r_1 and r_2 shown on the axes.

6. Conclusion

Though a combination of finite element methods and analytical solutions we have demonstrated that the particle shape that maximizes electrical torque is dependent on the ratio of particle permittivity to that of its environment ε_r. For a fixed particle length, particles with small values of ε_r experience maximum torque when their mass is concentrated towards the center, while particles with a larger value of ε_r realize their greatest torque with their mass distributed towards the ends of the particle. The results suggest that a magnetic core for the brachytherapy seed application described should be end-weighted.

References
[1]   Jones T B 1995 *Electromechanics of Particles* (New York: Cambridge)
[2]   Stratton J A 1941 *Electromagnetic Theory* (New York: McGraw-Hill)
[3]   McAleavey S A, Rubens D J and Parker K J 2003 Doppler ultrasound imaging of magnetically vibrated brachytherapy seeds *IEEE Trans Biomed Eng* **50** 252-5
[4]   McAleavey S A 2002 Doppler technique for the detection and localization of modified brachytherapy seeds" *Proc of SPIE* **4687** 190-198

Magnetically Vibrated Brachytherapy Seeds:

Ferromagnetic Core Models and Image Reconstruction Methods

Stephen A. McAleavey, Scott White, Manoj Menon
Department of Biomedical Engineering
University of Rochester
Rochester, NY., USA
stephenm@bme.rochester.edu

Abstract— **Magnetically Induced Motion Imaging (MIMI) uses an oscillating magnetic field and ultrasonic motion-tracking techniques to vibrate and identify brachytherapy seeds in situ. The efficacy of the technique relies on the ability to generate and detect seed vibration, and distinguish this vibration signal from other motion sources. The vibration of the seed depends on the torque generated by a ferromagnetic core in the seed. A design goal is to maximize the torque for the limited amount of core material that can be placed within a seed. We have developed 3D finite-element models for two seed core geometries, an ellipsoid and a rod capped by two semi-hemispheres. Both seed cores have identical volumes (7.4x10^{-10}m^3), length (4mm), and permeability (μ_r=4000). Calculation by the Maxwell Stress Tensor method yields a torque for the rod 1.4 times that of the ellipsoidal core, demonstrating the substantial sensitivity of torque on core geometry.**

The oscillating seeds act as dipole shear wave sources, with maximum vibration amplitude at the ends of the seed and a vibration minimum at the center of length. This gives rise to a characteristic vibration amplitude distribution in the surrounding tissue, with two lobes per seed. By taking advantage of the opposing phase of the seed ends, we demonstrate a method that links these lobes. A compounding technique for suppressing ring-down artifact is demonstrated. These methods are demonstrated on RF data acquired from seeds in beef muscle tissue. 3D vibration isosurface maps of seed vibration amplitude are presented and found to be in good agreement with previously reported simulations.

I. INTRODUCTION

We have previously reported a technique for imaging brachytherapy seeds called Magnetically Induced Motion Imaging (MIMI) [1,2]. Modified brachytherapy seeds containing a ferromagnetic core are made to oscillate about their center due to the time-varying torque induced on the cores. The vibration amplitude of the seed and surrounding tissue is on the order of 1 micron and is detected by ultrasonic motion tracking methods.

II. SEED CORE TORQUE

In the modified seeds the limited volume of the seed must be shared between the therapeutic radioisotope and the ferromagnetic core. The finite volume available to the core should be used as efficiently as possible to maximize the

torque on the seed, and thus its vibration, for a given magnetic field to improve sensitivity. The torque T on a ferromagnetic particle of isotropic permeability μ_r and volume V in a magnetic field of strength H_0 is a function of its shape [3], $T = -V\mu_0 H_0^2 \dfrac{\chi^2(L_{\parallel} - L_{\perp})}{(1 + \chi L_{\parallel})(1 + \chi L_{\perp})} c_x c_z$, where $L_{\perp}$ and $L_{\parallel}$ are shape functions and $\chi = \mu_r - 1$ the magnetic susceptibility. Torque may be calculated conveniently for the case of spheroids where analytical solutions for $L_{\perp}$ and $L_{\parallel}$ are known [3]. For a prolate spheroid with major to minor axis ratio $r = a/b$, the spheroid eccentricity is defined as $e = \sqrt{1 - 1/r^2}$, $L_{\parallel} = \dfrac{1}{2r^2 e^2}\left(\ln\left(\dfrac{1+e}{1-e}\right) - 2e\right)$ and $L_{\perp} = (1 - L_{\parallel})/2$. Torque versus r for a unit volume prolate spheroid in a unit field H is plotted Figure 1. In the limit as r tends to infinity $L_{\parallel} \to 0$ and $L_{\perp} \to 1/2$ so that the limiting value of T is $V\mu_0 H_0^2 \chi^2/(2+\chi)$. For a fixed length ellipsoid torque does not monotonically increase with r, as shown in Figure 2. For a fixed a, V increases as r decreases. For the dimensions of a brachytherapy seed, using the largest ellipsoid that fits in the seed maximizes torque.
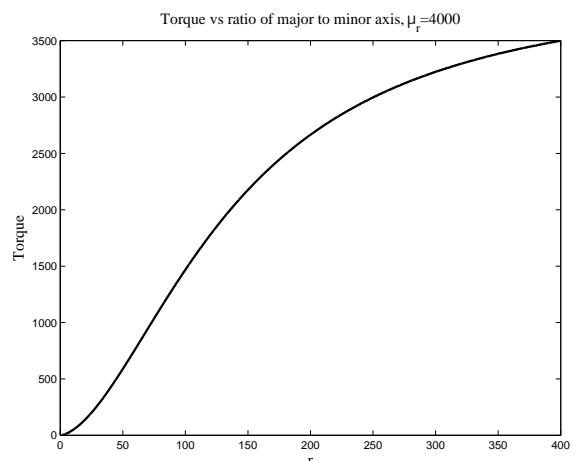

Figure 1. Torque increases monotonically for a constant volume ellipsoid as the ellipsoid transforms from spherical to highly eccentric.
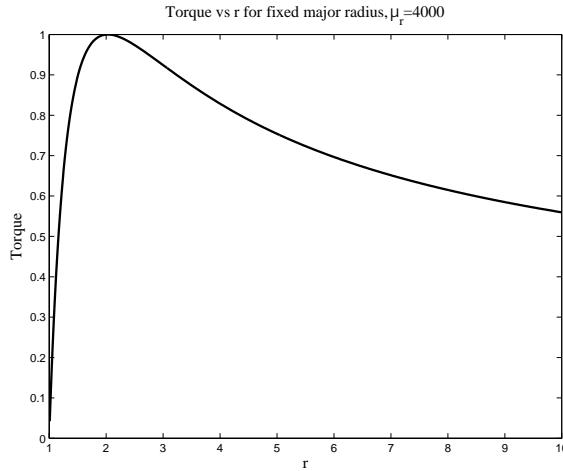
Figure 2. For a fixed length ellipsoid, the combination of varying volume and eccentricity give rise to a non-monotonic variation in torque. Typical brachytherapy seed dimensions imply that r can be no less than 10. Therefore the widest (largest b) ellipsoid that can be fit in the seed will maximize torque.

Clearly torque is a strong function of shape. To compute torque on non-spheroids a finite element model constructed using Comsol Multiphysics finite element software (Comsol, Inc. Burlington, MA). Spheroids and cylinders of identical volume ($7.4 \times 10\text{-}10$ m^3, one third the volume of a seed) were modeled [4]. These shapes were selected to allow straightforward comparison to analytical torque models. The flux B in the core material was modeled as linearly dependent on H, $B = \mu_0 \mu_r H$, with an isotropic relative permeability $\mu_r = 4000$. The torque exerted on the seed was calculated by the Maxwell Stress Tensor method [5]. Torque was calculated at a field value of $H = 1$A/m and scales as H^2. The finite-element calculated value for ellipsoid torque was $1.61 \times 10\text{-}14$Nm, in good agreement with the analytical value of $1.53 \times 10\text{-}14$Nm. The torque on the cylinder was calculated as $2.28 \times 10\text{-}14$Nm, ~1.4 times the torque of the ellipsoidal core.

III. SEED DETECTION

A. Experimental Method

Ferromagnetic seed cores were cut from 0.5mm diameter piano wire to a length of 5 mm. The seed cores were embedded in beef muscle tissue obtained from a local butcher. The seeds were induced to vibrate with a 13cm diameter coil of 200 turns of 18-gauge wire. The magnetic field at the center of the coil is given by $NI/2r$, where N is the number of turns, I the current, and r the coil radius. The maximum field value at the coil center was ~6,200 A/m at 50Hz. The measured resistance and inductance were 3ohms and 7.4mH. During scanning the axis of the coil was set at a 45° angle to the long axis of the seeds. The coil was driven by a 200W audio amplifier connected to a function generator at frequencies of 50 to 300Hz. RF echo data from the vibrating seeds and tissue were acquired using a Siemens Antares scanner and the Axius Direct Research Interface

with a VF10-5 linear array. The PRF of the Doppler sequence used was chosen to be 2.5-3 times the seed vibration frequency, within the available scanner settings. Three-dimensional RF data sets were acquired by translating the transducer in the elevational direction in 0.5mm increments.

Displacements were tracked using the 1D autocorrelation method of Kasai [6]. In contrast to standard Doppler tracking where phase shifts are averaged at a given depth over the Doppler ensemble, here phase shifts averaged in the axial direction over a distance of 1mm. Low frequency environmental vibration was removed by fitting and subtracting a linear component of displacement from the data. Vibration was quantified by calculating the RMS value of the remaining motion signal.

Figure 3a shows the measured coil current for a 500mV peak-peak amplifier current. The amplifier has a constant voltage gain, while torque is proportional to the square of current. Constant torque was maintained by adjusting the amplifier drive voltage to maintain constant current. Figure 3b shows vibration measured at the seed tip at 100 and 300 Hz with constant current drive. Vibration amplitude is on the order of 0.1 µm and roughly equal at each frequency.
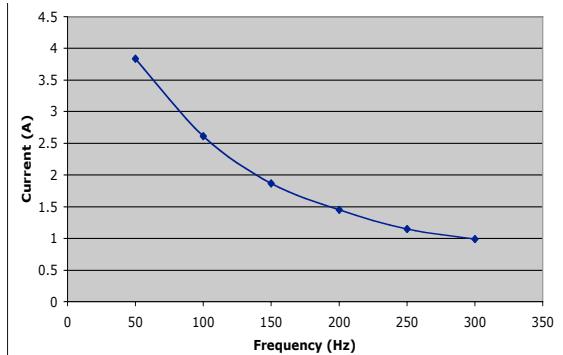

a
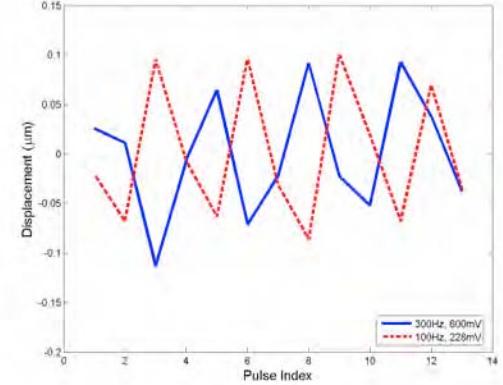
b

Figure 3. (a) Measured current in coil as a function of frequency for 500mVpp amplifier drive. As torque varies with the square of current, the vibration amplitude at 50Hz is ~16x larger than at 300Hz for constant input. (b) Measured seed tip displacements in beef tissue at 100 and 300Hz. Note the horizontal axis is pulse index, not time. The PRFs used were 610Hz and 1953Hz for the 100 and 300Hz signals. The input voltage was scaled to provide equal coil currents at both frequencies.

B. Synchronous detection and directional blurring

Synchronous detection of seed vibration was achieved by selecting the vibration frequency such that an integer number of cycles occur between Doppler ensembles. The displacement estimates $u(x,n)$ were then detected according to the relation $p(\vec{x}) = \sum_{n \in ensemble} u(\vec{x},n)\cos(2\omega_0 n / PRF)$, where ω_0 is the coil drive frequency, the vibration frequency being twice that due to the squared dependence of torque on current. The sign of p indicates whether the motion phase is 0° or 180°. The positive and negative components of p may be blurred in opposing directions to link the seed ends together, as illustrated in figure 5, allowing the seed to be segmented as a single object. The directionally blurred image was formed by creating two sub-images, $p_+(\vec{x}) = p(\vec{x})(p(\vec{x}) > 0)$ and $p_-(\vec{x}) = -p(\vec{x})(p(\vec{x}) \le 0)$, where the inequalities at a given x evaluate to 1 if true and 0 if false. These sub-images were convolved with filters possessing rightward and leftward bias (here a string of eight 1's followed by eight 0's and its reflection) and the results summed. In this way p_+ experiences a rightward blur while p_- experiences a leftward blur.

C. Ring down suppression:

Vibration amplitude isosurfaces generated from the 3D RF data often shows a ring-down artifact in the form of a "tail" distal to the seed, as in figure 6a. The ring-down tail is also evident in the displacement maps of figures 4 and 5. The tail appears in the image to proceed away from the seed in the direction of beam propagation, as acoustic energy continues to echo back from the reverberant seed. Changing the look direction by steering the ultrasound beam will cause the apparent location of the tail to change relative to the seed.

This tail may be eliminated by scanning from two or more look directions using the typical beam-steering control found in Color Doppler systems. The process is illustrated schematically in figure 7. Estimation of vibration amplitude is carried out on each data set independently. The data sets are thresholded to the isosurface value, and the product of the segmented volumes taken. As the location of the tail varies with steering angle while the seed location remains constant, the seeds are retained while the ring-down tails are suppressed.

This technique is demonstrated in Figures 6. Two parallel seeds embedded in beef tissue were scanned. Here the z axis represents the axial (beam) direction, the x axis the lateral image dimension, and y the out-of-plane dimension. The transducer was mounted on a three-axis positioner and moved in 0.5mm steps, while the seed was vibrated with the coil described above and an amplifier input of 600mVpp at 200Hz. The alignment of the seeds and transducer was selected to emphasize the ringdown artifact in the left-hand seed. Figure 6a illustrates the vibration amplitude isosurfaces generated for a straight-ahead (0° beam steering). The tails are clearly visible. Figure 8 was formed by collecting two echo data sets with beams steered at +/- 15°. Each displacement data set was segmented at the same isosurface value as figure 6a. The segmented volumes were

then multiplied on a voxel-by-voxel basis to arrive at the isosurface map shown in figure 6b.


(a)

(b)
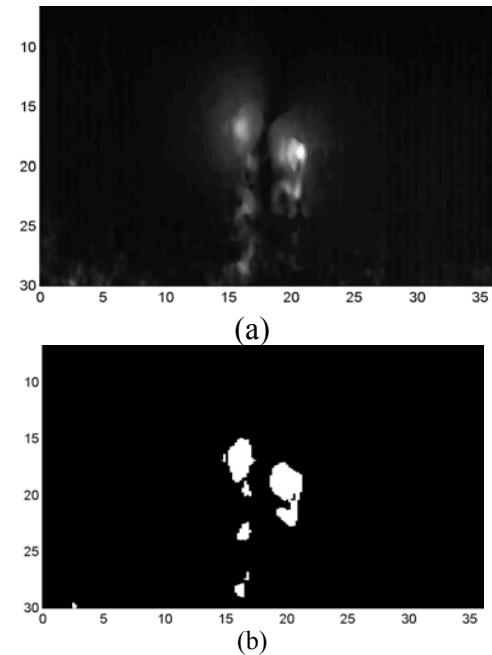
Figure 4. (a). Displacement map of estimated tissue displacement of seed in beef muscle. White represents 0.5μm RMS vibration amplitude, black 0μm. Note the dipole shape of the vibration field. (b) The vibration field thresholded at 0.3μm RMS.

(a)

(b)
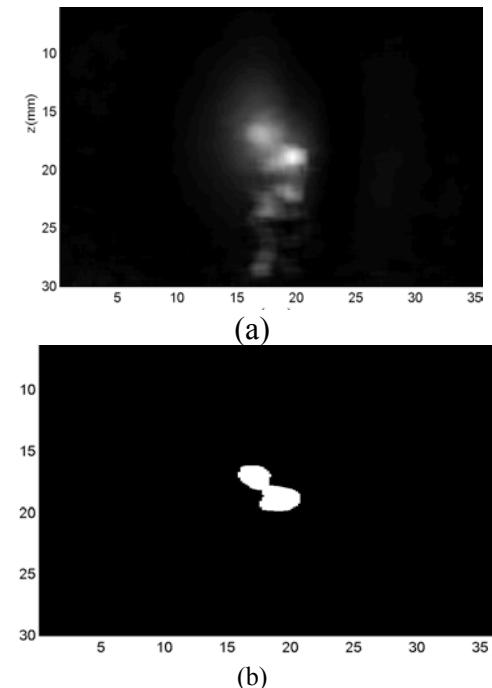
Figure 5. (a). Displacement map of estimated tissue displacement of seed in beef muscle following phase-sensitive blurring. White represents 0.5μm RMS vibration amplitude, black 0μm. Note the dipole shape of the vibration field. (b) The vibration field thresholded at 0.3μm RMS.
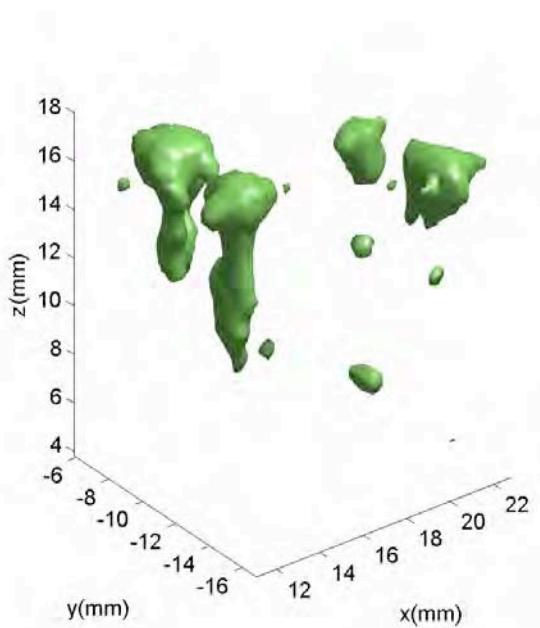
(a)
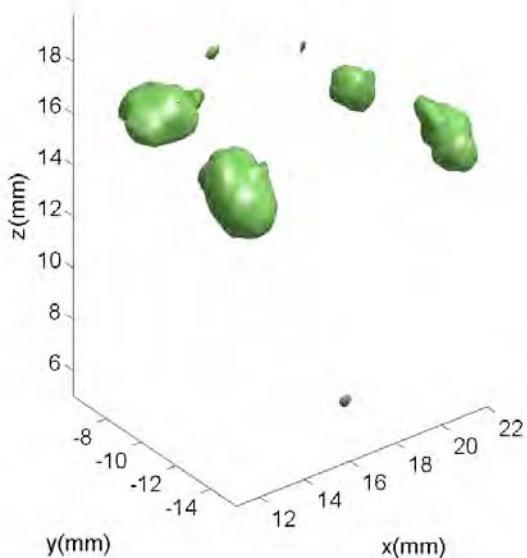
Figure 6(a) Seed isosurfaces calculated at 0.3μm RMS vibration amplitude at a beem angle of 0°. Note the ring down artifacts descending from the seeds. The transducer is at the top of the image at a hight of 32mm. (b) Vibration isosurfaces formed from multiplication (logical AND) of two segmented volumes acquired 30° apart. The ring down tails are effectively elliminated.
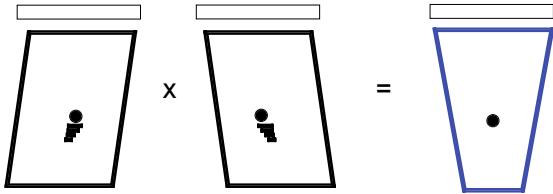

Figure 7. Schematic illustration of compounding method to suppress ring-down tails. Tails appear to radiate in the direction of beam propagation and change directioin as beam is steered, while the seed location remains constant regardless of steering angle. Multiplicatively combining multiple look directions eliminates tails and maintains seeds.

IV. CONCLUSION

Finite element calculations of torque on seed cores have been found to be in good agreement with known analytical solutions and allow extension to non-spheroidal geometries. Torque has been found to have substantial sensitivity to the shape of the ferromagnetic core. Further investigation and determination of an optimal core shape appears warranted.

Phase sensitive detection of seed vibration may be useful in segmenting seeds and linking opposing seed ends, overcoming the dark center in side-view seed segmentations due to the dipole nature of the vibration field. Ring down artifacts are common in images of brachytherapy seeds and may be effectively suppressed in vibration amplitude maps by multiplicative combination of multiple seed look angles.

REFERENCES

[1] S.A. McAleavey, M. Palmeri, S. Gracewski, G.E. Trahey, "Ferromagnetic Brachytherapy seed motion in soft tissue: Models, measurements and ultrasound detection," *Proceedings of the IEEE Ultrasonics Symposium*, pp. 1575-1579, 2002

[2] S.A. McAleavey, D.J. Rubens, K.J. Parker, "Doppler ultrasound imaging of magnetically vibrated brachytherapy seeds," *IEEE Transactions on Biomedical Engineering*, v 50, n 2, Feb 1, 2003, p 252-255

[3] T. B. Jones, Electromechanics of Particles, Cambridge, 1995

[4] *Electromagnetics Module User's Guide*, Comsol AB, 2004

[5] R.K. Wangsness, Electromagnetic Fields, John Wiley and Sons, 1986

[6] J.A. Jensen, *Estimation of Blood Velocities Using Ultrasound*, Cambridge,